Research Article

Nano Research
2023, 16(7): 9280–9288

ISSN 1998-0124 CN 11-5974/O4
https://doi.org/10.1007/s12274-023-5531-3

Highly active and durable triple conducting composite air electrode for low-temperature protonic ceramic fuel cells

Qi Huang[1,§], Shanshan Jiang[1,§] (✉), Yujia Wang[1], Jingjing Jiang[2] (✉), Yubo Chen[3], Jiahuan Xu[4], Hao Qiu[1], Chao Su[1], and Daifen Chen[1] (✉)

[1] *School of Energy and Power, Jiangsu University of Science and Technology, Zhenjiang 212100, China*
[2] *Institute of Analysis and Testing, Beijing Academy of Science and Technology (Beijing Center for Physical and Chemical Analysis), Beijing 100089, China*
[3] *School of Material Science and Engineering, Nanyang Technological University, 50 Nanyang Avenue, Singapore 639798, Singapore*
[4] *School of Science, Jiangsu University of Science and Technology, Zhenjiang 212100, China*
[§] *Qi Huang and Shanshan Jiang contributed equally to this work.*

Received: 3 December 2022 / **Revised:** 22 January 2023 / **Accepted:** 25 January 2023

ABSTRACT

Protonic ceramic fuel cells (PCFCs) are more suitable for operation at low temperatures due to their smaller activation energy (E_a). Unfortunately, the utilization of PCFC technology at reduced temperatures is limited by the lack of durable and high-activity air electrodes. A lot number of cobalt-based oxides have been developed as air electrodes for PCFCs, due to their high oxygen reduction reaction (ORR) activity. However, cobalt-based oxides usually have more significant thermal expansion coefficients (TECs) and poor thermomechanical compatibility with electrolytes. These characteristics can lead to cell delamination and degradation. Herein, we rationally design a novel cobalt-containing composite cathode material with the nominal composition of $Sr_4Fe_4Co_2O_{13+\delta}$ (SFC). SFC is composed of tetragonal perovskite phase ($Sr_8Fe_8O_{23+\delta}$, *I*4/*mmm*, 81 wt.%) and spinel phase (Co_3O_4, $Fd\bar{3}m$, 19 wt.%). The SFC composite cathode displays an ultra-high oxygen ionic conductivity (0.053 S·cm^{-1} at 550 °C), superior CO_2 tolerance, and suitable TEC value (17.01 × 10^{-6} K^{-1}). SFC has both the O^{2-}/e$^-$ conduction function, and the triple conducting (H^+/O^{2-}/e$^-$) capability was achieved by introducing the protonic conduction phase ($BaZr_{0.2}Ce_{0.7}Y_{0.1}O_{3-\delta}$, BZCY) to form SFC+BZCY (70 wt.%:30 wt.%). The SFC+BZCY composite electrode exhibits superior ORR activity at a reduced temperature with extremely low area-specific resistance (ASR, 0.677 Ω·cm^2 at 550 °C), profound peak power density (PPD, 535 mW·cm^{-2} and 1.065 V at 550 °C), extraordinarily long-term durability (> 500 h for symmetrical cell and 350 h for single cell). Moreover, the composite has an ultra-low TEC value (15.96 × 10^{-6} K^{-1}). This study proves that SFC+BZCY with triple conducting capacity is an excellent cathode for low-temperature PCFCs.

KEYWORDS

protonic ceramic fuel cells, spinel oxide, composition tuning, triple-conducting

1 Introduction

Energy generation through the utilization of renewable sources (wind, solar, and hydro) is constrained by the intermittent supply, thus leading to the mismatch between the power supply and demand. To avoid such problems, the development of innovative electrochemical energy storage and conversion technologies, such as metal air cells, fuel cells, and water splitting devices, has attracted considerable attention over the past few decades [1–5]. Among them solid oxide fuel cells (SOFCs) have been widely researched due to their high energy conversion efficiency, environmental friendliness, and adaptability to various fuels [6–9]. However, conventional SOFCs operate at very high temperatures (> 800 °C), which causes the difficulty of cell sealing, poor durability, and disappointing cell components' chemical compatibility, thus hindering the commercialization of this technology [10–14]. It is necessary to reduce the cell operating temperature to a low-temperature range (400–650 °C) while maintaining adequate power output [15–18]. To date, various methods have been explored to reduce the working temperature. One of the most extensively studied is the exploitation of new cathodes with higher oxygen reduction reaction (ORR) activity [19–22]. Compared with conventional SOFCs, protonic ceramic fuel cells (PCFCs) are more suitable for low-temperature applications because of two major advantages. On the one hand, the protonic conduction electrolyte has higher ionic conductivity than the oxygen ionic conduction electrolyte at reduced temperatures. On the other hand, water is generated on the cathode side of PCFCs, which can not only improve the fuel utilization rate, but also minimize the probability of nickel anode oxidation. Therefore, PCFCs have a better development prospect at low temperature [23–28]. However, the electrochemical performance of PCFCs is degraded mainly due to the high polarization impedance and low ORR activity of the cathode materials at low temperatures [29].

Cobalt-based perovskite materials with dual electronic and

Address correspondence to Shanshan Jiang, jss522@just.edu.cn; Jingjing Jiang, jiangjingjingnju@163.com; Daifen Chen, dfchen@just.edu.cn

ionic conductivity, such as $Sm_{0.5}Sr_{0.5}CoO_{3-\delta}$ (SSC), $Ba_{0.5}Sr_{0.5}Co_{0.8}Fe_{0.2}O_{3-\delta}$ (BSCF), and $La_{0.6}Sr_{0.4}CoO_{3-\delta}$ (LSC), are investigated as air electrodes for PCFCs, demonstrating good ORR activity and considerable power density [30–32]. However, their thermal expansion coefficients (TECs, 24×10^{-6}–32×10^{-6} K^{-1}) are higher than PCFCs electrolytes, such as $BaZr_{0.2}Ce_{0.7}Y_{0.1}O_{3-\delta}$ (BZCY, 10.1×10^{-6}–10.2×10^{-6} K^{-1}), because of the transition of Co^{3+} to Co^{4+} from the low spin to high spin [33]. Therefore, it is imperative and challenging to reduce TECs of cobalt-based perovskite. Zhang Yuan et al. have successfully reduced the TECs through the mechanism of thermal expansion compensation by introducing negative thermal expansion features [34]. However, the additional components often impede the charge transport in the electrode bulk. Cobalt-free perovskite oxides typically have more suitable TECs than cobalt-based perovskite, but generally exhibit lower ORR activity.

Spinel oxides possess high conductivity and good chemical compatibility with other ingredients, and have long been widely used in the protective coating on the metal interconnection layer of SOFCs. Recently they have been studied as feasible air electrode materials for SOFCs [35–39]. However, few studies have been conducted on spinel oxides as cathode materials of PCFCs. Cobalt spinel oxide materials have ideal TECs (11×10^{-6}–12.5×10^{-6} K^{-1}) and high electron conductivity. The low ionic conductivity of spinel structure is the main obstacle of the independently as a SOFC cathode material, which is more suitable for combining with other materials to prepare high-performance composite cathode, to take advantage of the tremendous thermal stability of spinel [39].

Here, we report a durable and high-performance triple conducting composite via composition tuning, serving as an air electrode for low-temperature PCFCs. During the simple and convenient calcination process, the $Sr_4Fe_4Co_2O_{13+\delta}$ (SFC) material with the nominal component of SFC intelligently self-assembles into two phases, the cobalt-free tetragonal perovskite phase $Sr_8Fe_8O_{23+\delta}$ (*I*4/*mmm*) and cobalt spinel phase Co_3O_4 ($Fd\bar{3}m$), respectively. We achieve SFC cathode with extremely low TEC values (17.01×10^{-6} K^{-1}) from the ordinary high TEC cobalt containing oxides. Besides that, The SFC cathode exhibits good ORR activity at reduced temperatures, achieved peak power density (PPD, 356 mW·cm^{-2} at 550 °C) with open-circuit voltage (OCV) of 1.081 V, affordable electronic conductivity (10.07 S·cm^{-1} at 550 °C), high oxygen ionic conductivity (0.053 S·cm^{-1} at 550 °C), and significant reversibility between pure air and air containing CO_2. And using a physical mixing method to introduce the protonic conduction composition into the SFC material with O^{2-}/e^- conduction function to synthesize a novel triple-conducting composite electrode (the SFC+BZCY). The SFC+BZCY composite electrode achieves the lowest area-specific resistance (ASR) of 0.677 Ω·cm^2 at 550 °C, and an extraordinarily high PPD of 535 mW·cm^{-2} at 550 °C with the OCV of 1.065 V. Moreover, the robust durability of the SFC+BZCY electrode is enabled 350 h for a single cell and over 500 h for a symmetrical cell operation.

2 Experimental

2.1 Materials synthesis and cell fabrication

SFC powder was rationally prepared by the sol-gel method. A stoichiometric amounts of $Sr(NO_3)_2$, $Fe(NO_3)_3{\cdot}9H_2O$, $Co(NO_3)_2{\cdot}6H_2O$, ethylenediaminetetraacetic acid, and citric acid were dissolved in the deionized water. The pH of the solution was adjusted to 7 by adding an appropriate amount of ammonia. The solution was keep stirred at a temperature of 80 °C until the solution turned to a transparent gel. The gel was heated at a temperature of 250 °C for 5 h to receive the precursor. And the precursor was further calcined at a temperature of 700 °C for 5 h under the control of oxygen partial pressure. The final SFC powder was obtained by calcining at 900 °C for 5 h under an ambient air atmosphere. Electrolyte powder BZCY was also prepared in the same method. The final phase formation temperature of the BZCY powder was controlled at 1100 °C.

The SFC was physically mixed with the BZCY at a proportional mass ratio of 7:3. Mixed powder was placed in a ball grinding tank with isopropanol, ethylene glycol, and propanetriol, and the ball grinding tank was ground for 2 h at 400 rpm. The electrolyte powder was placed in a die and the powder was pressed into a 15 mm diameter disk. Then, by sintering in an air atmosphere of 1450 °C for 5 h to obtain a dense electrolyte. To prepare symmetric cell, the mixed cathode slurry was evenly sprayed on the surface of electrolyte, and the silver layer was served as the flow collecting layer.

Ni+BZCY-supported single cells were prepared by co-pressing and co-firing. NiO powder was physically mixed with BZCY electrolyte powder and starch in a ratio of 6:4:1 to prepare the anode powder. The anode powder was pressed into the shape of a disk, and the appropriate amount of electrolyte powder was evenly spread on the disk and sintered at 1450 °C for 10 h for preparation of the half cell. The cathode slurry was sprayed on the electrolyte side of the half cell and prepared into an SFC+BZCY|BZCY|Ni+BZCY single cell.

2.2 Essential characterization and electrochemical testing

X-ray diffraction (XRD) instrument was used to explore the structure of the SFC sample. XRD diffraction instrument used Cu-K ray (wavelength λ = 1.5418 Å). The resulting XRD data with SFC powder was analyzed by GSAS refined software to obtain the unit cell parameters of the material. The conductivity of the cathode material was determined by the four-probe method. TEC of cathode materials was measured by Netsch DIL 402C/3/G thermal expansion instrument. The TEC was tested in air atmosphere from room temperature to 1000 °C. O_2 temperature-programmed desorption (O_2-TPD) was tested by a PCA1200 thermal weight analyzer. Scanning electron microscopy (SEM) was observed based on the cross-section of single cells.

The oxygen permeability was determined by gas chromatography (GC). The electrolyte powder was placed in a die and the powder was pressed into a 15 mm diameter disk to prepare thin disc. The thin disc was placed in a high-temperature furnace and calcined at 1100 °C for 5 h, before grinding both sides of the thin disc until a thickness of 1 mm. The thin disc was sealed on the side of the quartz pipe with conductive glue and placed in the test furnace. Argon was fed into the quartz pipe to exclude air, then oxygen passing through the disc was collected and sent into the chromatograph for analysis. The oxygen ion conductivity of the SFC cathodes could be determined from the oxygen permeation flux and the calculation methods are shown in Ref. [40].

Electrochemical impedance spectroscopy (EIS) was one of the common methods used to study the electrode polarization impedance and the electrolyte ohmic impedance. Prinston impedance spectrum analyzer was used to obtain EIS, measurement frequency range of 1 MHz–0.01 Hz, stable AC signal amplitude of 10 mV, and temperature range of 400–650 °C. Fitting analysis of the EIS was performed by the ZView software. And the obtained spectra were further analyzed by the distribution of relaxation time (DRT) technology using a MATLAB tool developed by Ciucci et al. [41]. When testing the current–voltage (*I*–*V*) and current–power (*I*–*P*) curves of a single cell, the anode-supported single cell was packaged at the quartz pipe, with H_2 as

the fuel on the anode side, and the flow rate was controlled at 80 mL·min^{-1} [STP] through the mass flow meter. The cathode side was exposed to the external air, and the ambient air was an oxidant. The cell test temperature was 400–650 °C, and the test instrument was Keithley 2460 digital power supply meter.

3 Results and discussion

X-ray diffraction was used to explore the phase compositions of the SFC sample. The XRD data were further analyzed by GSAS refinement software. As illustrated in Fig. 1(a), the as-prepared SFC oxide consists of two crystal phases, tetragonal perovskite phase $Sr_8Fe_8O_{23+\delta}$ (*I*4/*mmm*) and spinel phase Co_3O_4 ($Fd\bar{3}m$), respectively. According to the Rietveld refinement results, the tetragonal perovskite structure with lattice parameter $a = b =$ 10.9354 Å and c = 7.7040 Å (81 wt.%), the spinel perovskite structure with lattice parameter $a = b = c$ =8.2599 Å (19 wt.%), and the refinement reliability factors were R_p = 3.20%, R_{wp} = 4.08%, and χ^2 = 1.341. The formation of the $Sr_8Fe_8O_{23+\delta}$ and Co_3O_4 in the SFC sample was also observed by a high-resolution transmission electron microscopy (HR-TEM). Two lattice spacings demonstrated in Fig. 1(b) were 0.253(3) nm and 0.294(5) nm, corresponding to the (440) lattice plane of $Sr_8Fe_8O_{23+\delta}$ and (422) lattice plane of Co_3O_4, respectively. The existence of nanoscale spinel oxide Co_3O_4 is detected. The spinel phase Co_3O_4 and tetragonal perovskite phase $Sr_8Fe_8O_{23+\delta}$ were connected very well.

Undoubtedly, the electron and oxygen ionic conductivity of cathode materials play an important role in ORR activity. The electron conductivity of the SFC sample was tested using a four-probe DC technique. The test results are shown in Fig. 2(a), the electron conductivity of SFC is above 6.5 S·cm^{-1} at the temperature range from 400 to 650 °C, and the electron conductivity increases with increasing temperature, up to 12 S·cm^{-1}. The oxygen permeability was determined by GC, and the oxygen ionic conductivity was calculated and shown in Fig. 2(b), at 400–650 °C, increasing from 0.006 to 0.095 S·cm^{-1}. The oxygen ionic conductivity of SFC (0.095 S·cm^{-1} at 650 °C) reported here shows a significant advantage over some high-activity PCFCs cathodes, such as $BaCo_{0.7}(Ce_{0.8}Y_{0.2})_{0.3}O_{3-\delta}$ (BCCY, 0.04 S·cm^{-1} at 650 °C) and $Ba_{0.95}Ca_{0.05}Fe_{0.9}Y_{0.1}O_{3-\delta}$ (BCYF, 0.06 S·cm^{-1} at 650 °C) [42, 43]. These results reveal that the SFC is an excellent mixed ionic and electronic conductor (MIEC), representing the potential of SFC as a PCFC cathode.

The operational stability of the PCFCs is mainly related to the CO_2 tolerance of the cathode material and thermal compatibility between the fuel cell components. Due to the presence of CO_2 in ambient air (about 0.03%), the tolerance of the cathode to CO_2 poisoning is crucial for the practical application of PCFCs. Typically, CO_2 reacts with cations on the cathode surface to form a carbonate, thereby covering the active site and reducing the ORR activity. The CO_2 tolerance of the SFC cathode is investigated by changing the test environment of the SFC|BZCY|SFC symmetric cell (from wet air to wet air containing 1% CO_2 to wet air of removed 1% CO_2), and the results are shown in Fig. 3(a). The ASR values were increased from 0.83 to 1.78 Ω·cm^2 when 1% CO_2 was introduced, probably owing to the competitive adsorption of CO_2 to O_2 at active sites [44]. However, after the removal of CO_2, the ASR values were instantly decreased to the initial state, indicating remarkable reversibility of the SFC material between pure air and air containing CO_2, which may be attributed to the outstanding stability of the spinel oxide against CO_2 [45]. Stabilize for 200 min, and the ASR value is found to stabilize at about half of the initial value, as shown in Fig. 3(b). This phenomenon is consistent with the test results of Gu et al. [46], which can be attributed to the CO_2-induced carbonate formation and decomposition leading to the surface reconstruction, resulting in a significant improvement of the charge transfer process for ORR.

EIS spectra of symmetrical cells with a configuration of SFC|BZCY|SFC measured at 450–650 °C are shown in Fig. 3(c), and the ASR values of the symmetrical cells with the SFC cathode were 0.26, 0.65, 1.81, and 5.73Ω·cm^2 at 650, 600, 550, and 500 °C, respectively. The SFC|BZCY|Ni+BZCY single cell obtains power density, as shown in Fig. 3(d). At 650, 600, 550, 500, 450, and 400 °C, the PPD of SFC-based PCFCs is 502, 444, 356, 263, 193, and 154 mW·cm^{-2}, respectively. Corresponding OCV is 1.033, 1.06, 1.081, 1.094, 1.115, and 1.122 V, approximating the theoretical values calculated through the Nernst equation, which proves the rationality of the above experimental results. Figure S1 in the Electronic Supplementary Material (ESM) gives the cross-section image of the SFC|BZCY|Ni+BZCY single cell, and BZCY electrolyte with a thickness of ~ 20 μm.

Triple conducting composite cathode was evaluated to optimize the performance of PCFCs. By introducing protonic conductor BZCY into the SFC cathode, the proton could be transported from the electrolyte to the cathode, thus extending the active center from the TPB to the entire cathode, and greatly enhancing the ORR activity. Therefore, the SFC+BZCY composite cathode was prepared by physically mixing the SFC and the BZCY powder with a 7:3 mass ratio.

To evaluate the effect of the introduced protonic conductor on the oxygen desorption capacity of cathode materials, O_2-TPD was estimated for SFC, SFC+BZCY, and BZCY oxides, and the O_2-TPD plots are shown in Fig. 4(a). For the SFC, SFC+BZCY, and BZCY oxides under the rising temperature in an argon atmosphere, the B-site metal ions with variable valence in the samples were thermally reduced, accompanied by lattice oxygen desorption. Two oxygen desorption peaks corresponded to α oxygen at the lower temperature zone (200–450 °C) and β oxygen

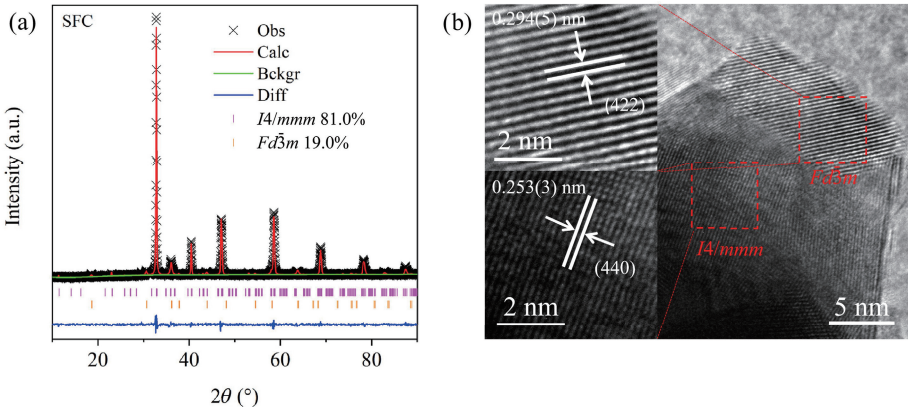

Figure 1 (a) Refined XRD profile of SFC sample. (b) HR-TEM image of SFC sample.

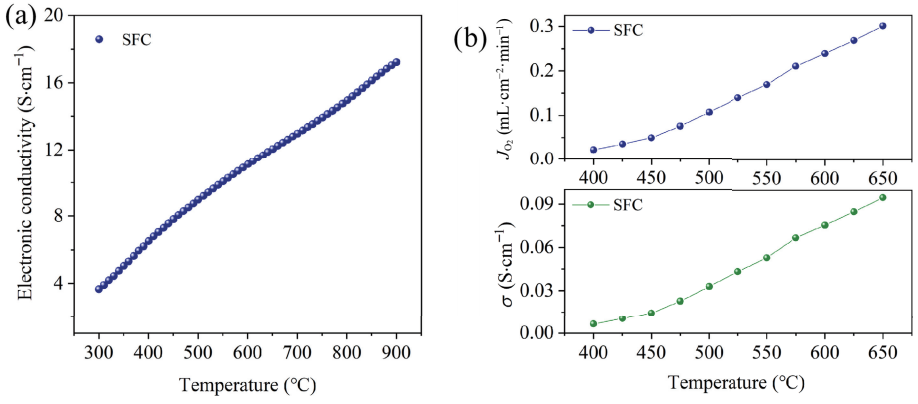

Figure 2 (a) Electron conductivity of the SFC. (b) Oxygen permeation flux and oxygen ionic conductivity for membranes made of SFC.

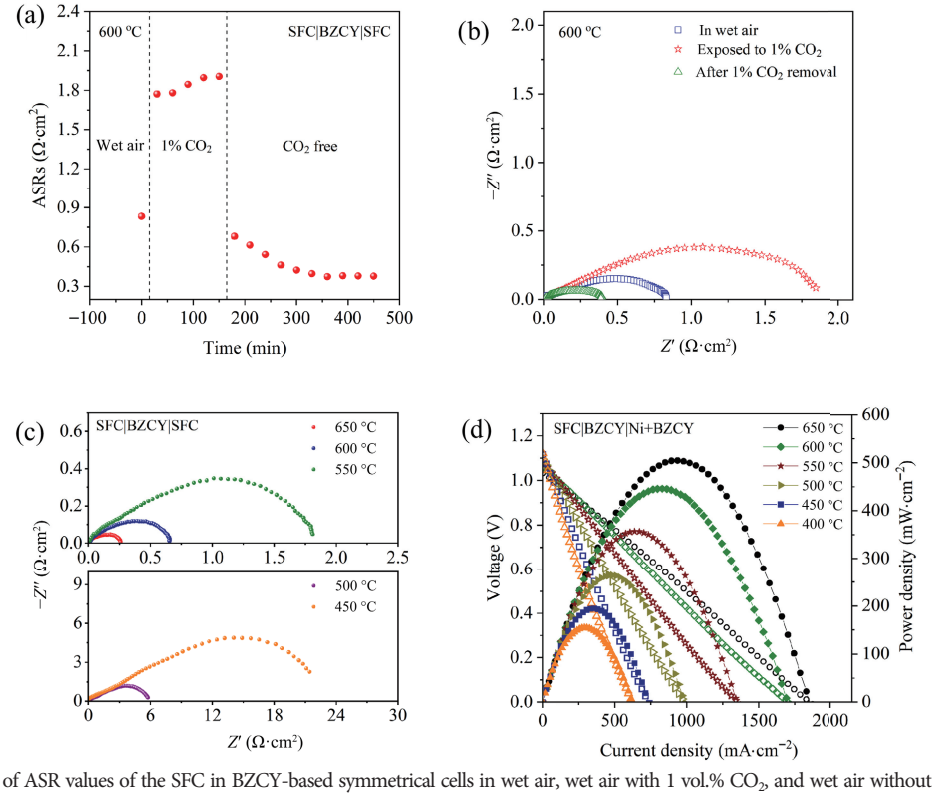

Figure 3 (a) Evolution of ASR values of the SFC in BZCY-based symmetrical cells in wet air, wet air with 1 vol.% CO_2, and wet air without CO_2 at 600 °C . (b) EIS curves of BZCY-supported symmetrical cells with SFC cathodes tested under different atmospheres at 600 °C. (c) EIS spectra of SFC electrode measured at 450–650 °C. (d) *I*–*V* and power density curves of PCFC with the configuration of SFC|BZCY|Ni+BZCY at 400–650 °C.

at the higher temperature zone (550–900 °C), respectively. The onset desorption temperatures for α oxygen of the SFC+BZCY were significantly lower than those of the SFC, suggesting that the introduced protonic conductor reduces the initiation temperature of oxygen desorption. Moreover, SFC+BZCY has the highest β oxygen desorption degree, suggesting the reduction of the transition metal ions was significantly facilitated by the addition of BZCY, indicating the SFC+BZCY electrolyte has increased oxygen mobility.

The thermal mismatch between the cathode and the electrolyte results in a sizeable internal strain and thus triggers a severe degradation and stratification of the PCFCs. In this work, the TEC of SF ($Sr_8Fe_8O_{23+\delta}$), SFC, and SFC+BZCY cathode materials is thoroughly investigated. As shown in Fig. 4(b), at the temperature range of 50–800 °C, the average TEC values of the SF and SFC are 31.90×10^{-6} and 17.01×10^{-6} K^{-1}, respectively. The SF shows a high TEC value, thereby the gigantic thermal expansion offset of SFC composite is mainly ascribed to the existence of cobalt spinel phase (19 wt.%). The average TEC value of the SFC+BZCY triple conducting composite is ultra-low, only 15.96×10^{-6} K^{-1}, which is much less than the reported TEC values of classical cobalt-containing cathode materials.

EIS can directly reflect the ORR activity of the cathode materials. This work evaluated the effect of introducing the protonic conductor on the ORR activity of the SFC cathode by comparing the ASRs of the SFC with the SFC+BZCY. Symmetric cells SFC|BZCY|SFC and SFC+BZCY|BZCY|SFC+BZCY were prepared and subjected to the electrochemical impedance test. Arrhenius plots displayed in Fig. 4(c) indicate that the impedance of the SFC+BZCY-based symmetric cells is significantly below the SFC. Moreover, the activation energy (E_a) of the SFC+BZCY (120.67 kJ·mol^{-1}) was also slightly lower than that of the SFC (123.04 kJ·mol^{-1}). The introduction of a protonic conductor greatly enhanced the ORR activity of the cathode material and reduced the activation energy of the material. Table S1 in the ESM gives specific ASR values of the symmetrical cell with the SFC+BZCY as electrode, and the ASR values were 0.68 Ω·cm^2 at 550 °C, which is only 37% of the value obtained for the SFC cathode at the same temperature.

The R_{ohm}-(R_{E1}-CPE1)-(R_{E2}-CPE2) equivalent circuit was used to

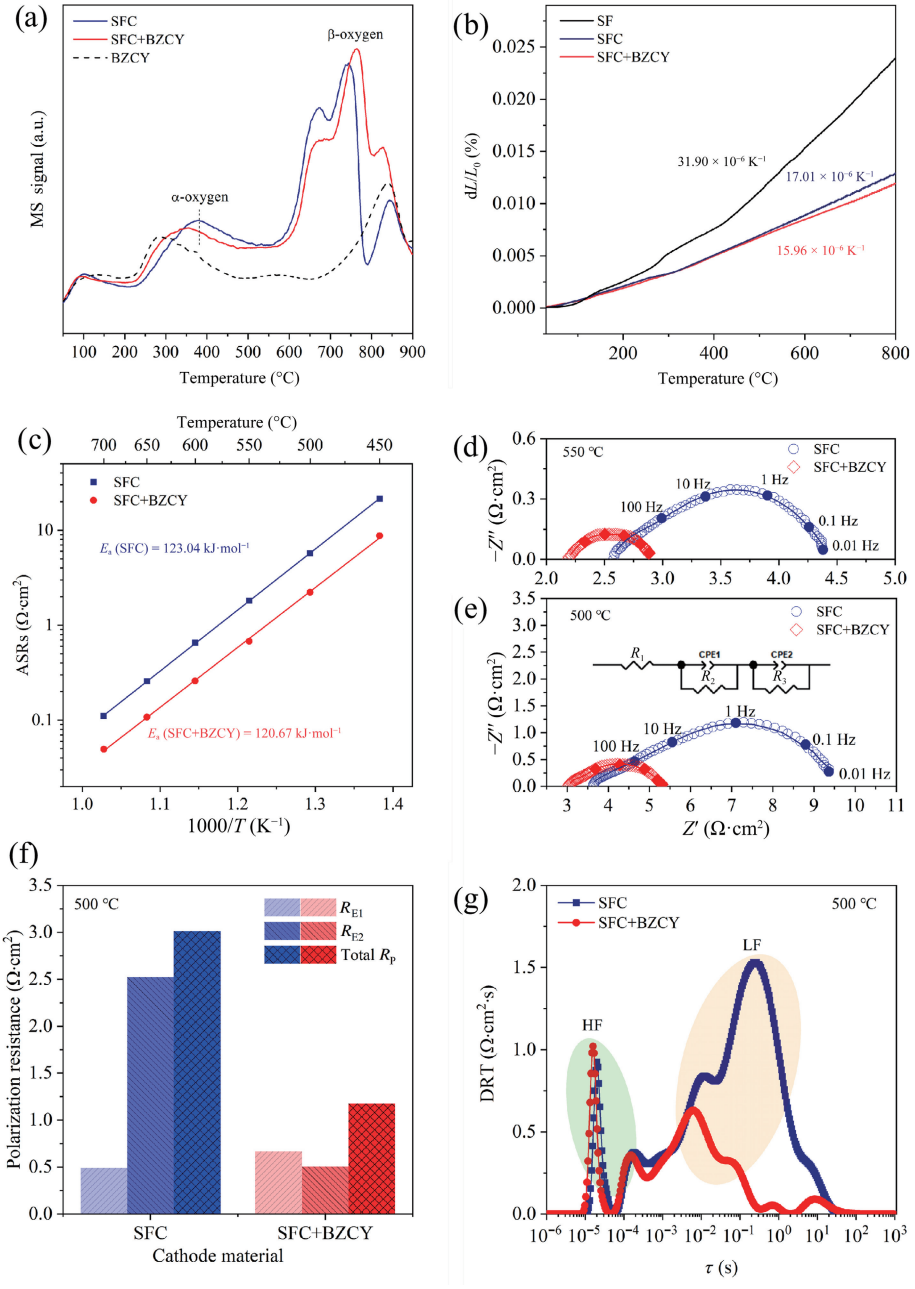

Figure 4 (a) O_2-TPD plots of SFC, SFC+BZCY, and BZCY. (b) TEC curves of the SF, SFC, and SFC+BZCY. (c) The Arrhenius plots of the ASR of the cathode materials of SFC and SFC+BZCY at different temperatures. (d) and (e) Fitting diagrams of symmetric cells based on SFC and SFC+BZCY cathode materials at 500 and 550 °C. (f) Bar graph of R_{E1} and R_{E2} of the cathode materials SFC and SFC+BZCY at 500 °C. (g) The DRT analysis plot of the EIS data of the SFC and SFC+BZCY at 500 °C.

fit the EIS data as shown in Figs. 4(d) and 4(e). The R_{ohm} is mainly related to the ohmic impedance of the cell. R_{E1} and R_{E2} represent the charge transfer process and the oxygen surface exchange process, respectively. Figure 4(f) shows the fitting results of R_{E1} and R_{E2} for the two cathodes at 500 °C, with the R_P being the sum of R_{E1} and R_{E2}. The fitting results showed that the R_{E1} of the SFC+BZCY was slightly larger than the SFC. At the same time, the R_{E2} of the SFC+BZCY was exceedingly more minor than the SFC single cathode at 500 °C, which indicates that the addition of the BZCY electrolyte slightly hindered electron conduction, but significantly accelerated the oxygen surface process. Overall, adding BZCY electrolyte powder is an effective method to reduce the polarization resistance of the material and enhance the ORR activity, which may be assigned to the triple conductivity capability of the SFC+BZCY composite cathode.

To further investigate the promoting effects of introducing the protonic conductor on the ORR activity of the SFC cathode, the DRT technology has been used to analyze the obtained EIS data as shown in Fig. 4(g). The high frequency (HF) and low frequency (LF) regions are shown, and the HF and LF represent the charge transfer process and the oxygen surface exchange process, respectively. It is found that the peak of HF for the SFC+BZCY composite cathode is slightly higher than that of the SFC single cathode. The peak intensity of LF for SFC+BZCY is much lower than that of the SFC cathode, which suggests that although the introduction of a protonic conductor hinders the charge transfer, it dramatically improves the oxygen surface exchange process, which is inconsistent with the results of EIS fitting analysis.

Figure 5(a) illustrates the impedance spectra of symmetrical cells with a configuration of SFC+BZCY|BZCY|SFC+BZCY measured at 450–650 °C. Furthermore, SFC+BZCY symmetrical cell exhibited excellent long-term durability, as shown in Fig. 5(b), and the ASR value of the symmetric cell increased at a rate of 1.5 × 10^{-4} Ω·cm²·h^{-1} during 500 h in the air atmosphere at 550 °C. The

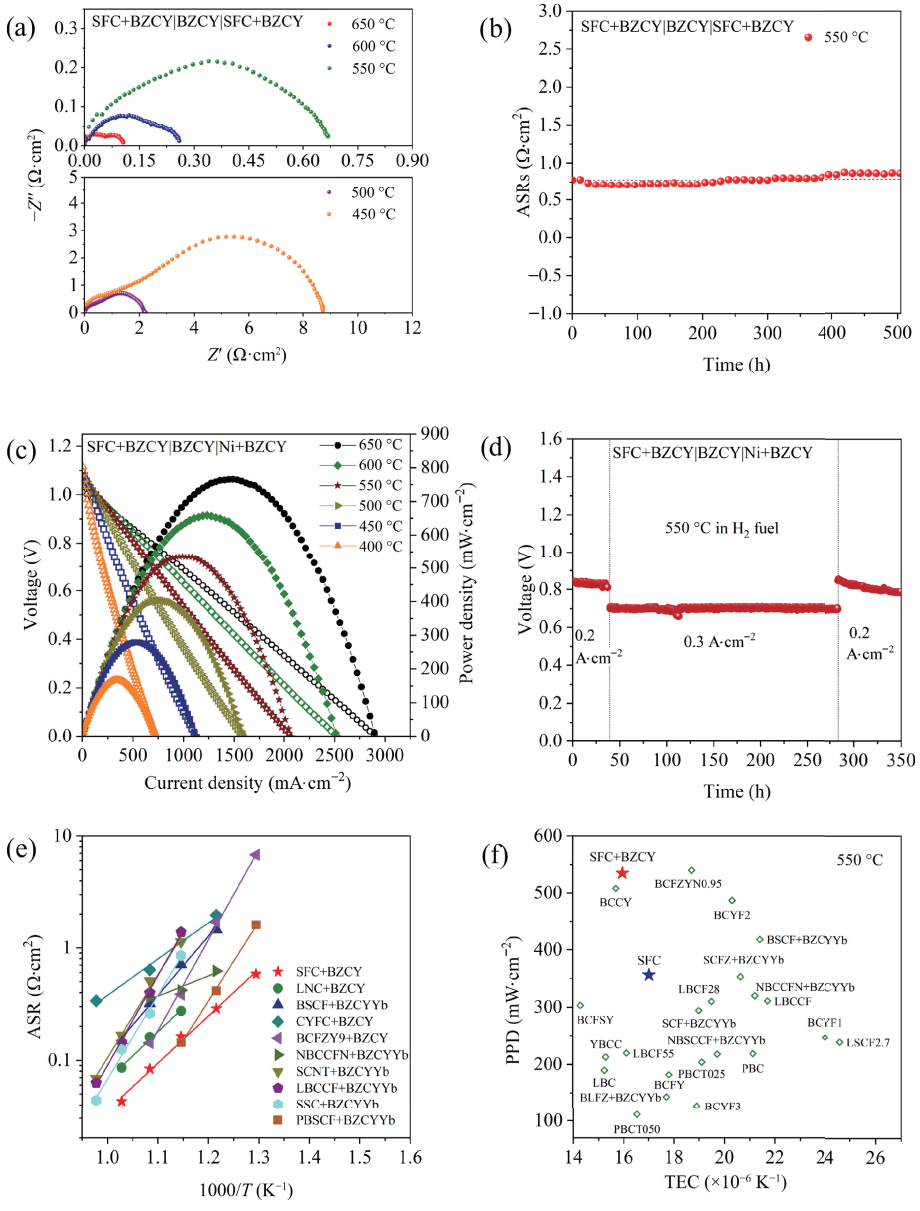

Figure 5 (a) EIS curves of symmetrical cell with SFC+BZCY as air electrode measured at 450–650 °C. (b) Stability diagram of the symmetric cell with SFC+BZCY as air electrode at 550 °C. (c) *I*–*V* and power density curves of PCFC with SFC+BZCY as air electrode at 450–650 °C. (d) Stability of PCFC with the structure of SFC+BZCY|BZCY|Ni+BZCY at constant current densities of 0.2 and 0.3 A·cm^{-2} at 550 °C. (e) The ASR values obtained by SFC+BZCY composite cathode compared with other reported composite cathodes with protonic electrolytes in PCFCs. (f) The comparison mapping of TEC and PPD for SFC and SFC+BZCY with the recently well-known cathodes at 550 °C.

SFC+BZCY composite cathode has exceedingly good operating stability, assigned to the extremely low TEC of the composite cathode material.

Figure 5(c) gives the electrochemistry performance of SFC+BZCY|BZCY|Ni+BZCY single cell. Under similar test conditions, the PPD of PCFCs for the SFC+BZCY is 766, 659, 535, 403, 278, and 167 mW·cm^{-2}, and the corresponding OCV is 1.012, 1.048, 1.065, 1.08, 1.094, and 1.116 V, at 650, 600, 550, 500, 450, and 400 °C. It indicates that the appropriate amount of BZCY powder introduced in the SFC cathode material is an effective way to optimize cell performance. This positive result should be owing to the $H^+/O^{2-}/e^-$ triple conductivity capability extending the active center from the TPB to the entire cathode, thus increasing ORR activity sites. The output performance of PCFCs, whether based on a single cathode or composite cathode, is better than the many well-known cathode materials [47–66].

Furthermore, the single cell for the SFC+BZCY showed exceeding operational stability, as shown in Fig. 5(d). During the 350 h test period, no significant cell performance decline was observed at a test temperature of 550 °C. Figure S2 in the ESM shows the SEM diagram of the cross-section of the SFC+BZCY|BZCY|Ni+BZCY single cell after the duration test, containing the porous cathode, dense BZCY electrolyte (~ 25 μm), and Ni+BZCY composite anode three layers. The adhesion between the cathode and the BZCY electrolyte is tight, signifying the thermal compatibility of the two layers.

The ASR values obtained by SFC+BZCY composite cathode compared with other reported composite cathodes with protonic electrolytes in PCFCs [40] are shown in Table S2 in the ESM. The TEC and corresponding PPD values of various cathode materials based on PCFCs were summarized, the comparison mapping is shown in Fig. 5(f), and the specific values are listed in Table S3 in the ESM. The comparison mapping revealed the SFC and SFC+BZCY cathode materials exhibit excellent electrochemical properties as well as a sufficiently low thermal expansion coefficient [28, 42, 43, 51, 54, 56, 58–66].

4 Conclusions

In summary, the SFC cathode has been synthesized via self-assembled. SFC is composed of a tetragonal perovskite phase (mass ratio 81 wt.%) and a spinel phase (19 wt.%). In addition, the SFC cathode has outstanding CO_2 tolerance, superior oxygen ionic conductivity, and ultra-low TEC. And the PPD value of SFC-based PCFC was 356 mW·cm^{-2} at 550 °C. The triple-conducting composite cathode was prepared by introducing protonic conducting capability into the SFC cathode via physically mixing the SFC cathode and the BZCY electrolyte at a 7:3 mass ratio. And expanding ORR active sites from TPB to the entire cathode region, thus effectively promoting the oxygen ion migration rate and improving the oxygen surface process. As for PCFCs performance, the SFC+BZCY cathode takes an excellent PPD of 535 mW·cm^{-2} at 550 °C, 50% higher than the SFC cathode. At the same time, the SFC+BZCY cathode showed an exceeding long-term operational durability (symmetric cell for over 500 h at 550 °C and the single cell for 350 h at 550 °C). These studies reveal that SFC+BZCY is a highly active and durable triple-conducting composite air electrode material for low-temperature PCFCs.

Acknowledgements

This research was financially supported by the National Natural Science Foundation of China (No. 22179054), the National Natural Science Foundation of China (No. 22101150), Natural Science Foundation of Jiangsu Province, China (No. BK20190965), and Natural Science Foundation of the Jiangsu Higher Education Institutions of China (No. 18KJB470011).

Electronic Supplementary Material: Supplementary material (cross-section SEM images, specific ASRs values, ASRs values comparison table, and summary of PPD and TEC) is available in the online version of this article at https://doi.org/10.1007/s12274-023-5531-3.

References

[1] Wang, Y.; Zheng, M.; Li, Y. R.; Ye, C. L.; Chen, J.; Ye, J. Y.; Zhang, Q. H.; Li, J.; Zhou, Z. Y.; Fu, X. Z. et al. p-d orbital hybridization induced by a monodispersed Ga site on a Pt_3Mn Nanocatalyst boosts ethanol electrooxidation. *Angew. Chem., Int. Ed.* **2022**, *61*, e202115735.

[2] Cui, T. T.; Wang, Y. P.; Ye, T.; Wu, J.; Chen, Z. Q.; Li, J.; Lei, Y. P.; Wang, D. S.; Li, Y. D. Engineering dual single-atom sites on 2D ultrathin N-doped carbon nanosheets attaining ultra-low-temperature zinc-air battery. *Angew. Chem., Int. Ed.* **2022**, *61*, e202115219.

[3] Zheng, X. B.; Yang, J. R.; Xu, Z. F.; Wang, Q. S.; Wu, J. B.; Zhang, E. H.; Dou, S. X.; Sun, W. P.; Wang, D. S.; Li, Y. D. Ru-Co pair sites catalyst boosts the energetics for the oxygen evolution reaction. *Angew. Chem., Int. Ed.* **2022**, *61*, e202205946.

[4] Jiang, J. J.; Jiang, P.; Wang, D. S.; Li, Y. D. The synthetic strategies for single atomic site catalysts based on metal-organic frameworks. *Nanoscale* **2020**, *12*, 20580–20589.

[5] Jiang, S. S.; Liu, Y.; Qiu, H.; Su, C.; Shao, Z. P. High selectivity electrocatalysts for oxygen evolution reaction and anti-chlorine corrosion strategies in seawater splitting. *Catalysts* **2022**, *12*, 261.

[6] Su, C.; Wang, W.; Shao, Z. P. Cation-deficient perovskites for clean energy conversion. *Acc. Mater. Res.* **2021**, *2*, 477–488.

[7] Yang, G. M.; Su, C.; Shi, H. G.; Zhu, Y. L.; Song, Y. F.; Zhou, W.; Shao, Z. P. Toward reducing the operation temperature of solid oxide fuel cells: Our past 15 years of efforts in cathode development. *Energy Fuels* **2020**, *34*, 15169–15194.

[8] Belotti, A.; Liu, J. P.; Curcio, A.; Wang, J.; Wang, Z.; Quattrocchi, E.; Effat, M. B.; Ciucci, F. Introducing Ag in $Ba_{0.9}La_{0.1}FeO_{3-\delta}$: Combining cationic substitution with metal particle decoration. *Mater. Rep.: Energy* **2021**, *1*, 100018.

[9] Ma, Z. L.; Li, L.; Ye, Q. R.; Dongyang, B. K.; Yang, W. Y.; Dong, F. F.; Lin, Z. Facile approach to enhance activity and CO_2 resistance of a novel cobalt-free perovskite cathode for solid oxide fuel cells. *ACS Appl. Mater. Interfaces* **2022**, *14*, 30881–30888.

[10] Bi, L.; Shafi, S. P.; Da'as, E. H.; Traversa, E. Tailoring the cathode–electrolyte interface with nanoparticles for boosting the solid oxide fuel cell performance of chemically stable proton-conducting electrolytes. *Small* **2018**, *14*, 1801231.

[11] Liu, Z. Q.; Chen, Y.; Yang, G. M.; Yang, M. T.; Ji, R. F.; Song, Y. F.; Ran, R.; Zhou, W.; Shao, Z. P. One-pot derived thermodynamically quasi-stable triple conducting nanocomposite as robust bifunctional air electrode for reversible protonic ceramic cells. *Appl. Catal. B: Environ.* **2022**, *319*, 121929.

[12] Teng, Z. Y.; Xiao, Z. R.; Yang, G. M.; Guo, L.; Yang, X. Q.; Ran, R.; Wang, W.; Zhou, W.; Shao, Z. P. Efficient water splitting through solid oxide electrolysis cells with a new hydrogen electrode derived from A-site cation-deficient $La_{0.4}Sr_{0.55}Co_{0.2}Fe_{0.6}Nb_{0.2}O_{3-\delta}$ perovskite. *Mater. Today Energy* **2020**, *17*, 100458.

[13] Carneiro, J.; Nikolla, E. Nanoengineering of solid oxide electrochemical cell technologies: An outlook. *Nano Res.* **2019**, *12*, 2081–2092.

[14] Duan, N. Q.; Yang, J. J.; Gao, M. R.; Zhang, B. W.; Luo, J. L.; Du, Y. H.; Xu, M. H.; Jia, L. C.; Chi, B.; Li, J. Multi-functionalities enabled fivefold applications of $LaCo_{0.6}Ni_{0.4}O_{3-\delta}$ in intermediate temperature symmetrical solid oxide fuel/electrolysis cells. *Nano Energy* **2020**, *77*, 1050207.

[15] Evans, A.; Martynczuk, J.; Stender, D.; Schneider, C. W.; Lippert, T.; Prestat, M. Low-temperature micro-solid oxide fuel cells with partially amorphous $La_{0.6}Sr_{0.4}CoO_{3-\delta}$ Cathodes. *Adv. Energy Mater.* **2015**, *5*, 1400747.

[16] Kuai, X.; Yang, G. Y.; Chen, Y. B.; Sun, H. N.; Dai, J.; Song, Y. F.; Ran, R.; Wang, W.; Zhou, W.; Shao, Z. P. Boosting the activity of $BaCo_{0.4}Fe_{0.4}Zr_{0.1}Y_{0.1}O_{3-\delta}$ perovskite for oxygen reduction reactions at low-to-intermediate temperatures through tuning B-site cation deficiency. *Adv. Energy Mater.* **2019**, *9*, 1902384.

[17] Gu, H. X.; Yang, G. M.; Hu, Y.; Liang, M. Z.; Chen, S. H.; Ran, R.; Xu, M. G.; Wang, W.; Zhou, W.; Shao, Z. P. Enhancing the oxygen reduction activity of $PrBaCo_2O_{5+\delta}$ double perovskite cathode by tailoring the calcination temperatures. *Int. J. Hydrogen Energy* **2020**, *45*, 25996–26004.

[18] Cai, C. K.; Xie, M. Y.; Xue, K.; Shi, Y.; Li, S. T.; Liu, Y. Y.; An, S. L.; Yang, H. Enhanced electrochemical performance of $La_{0.6}Sr_{0.4}Co_{0.2}Fe_{0.8}O_{3-\delta}$ cathode via Ba-doping for intermediate-temperature solid oxide fuel cells. *Nano Res.* **2022**, *15*, 3264–3272.

[19] Zhuang, Z. C.; Li, Y. H.; Yu, R. H.; Xia, L. X.; Yang, J. R.; Lang, Z. Q.; Zhu, J. X.; Huang, J. Z.; Wang, J. O.; Wang, Y. et al. Reversely trapping atoms from a perovskite surface for high-performance and durable fuel cell cathodes. *Nat. Catal.* **2022**, *5*, 300–310.

[20] Zhang, S. L.; Liu, T.; Li, C. J.; Yao, S. W.; Li, C. X.; Yang, G. J.; Liu, M. L. Atmospheric plasma-sprayed $La_{0.8}Sr_{0.2}Ga_{0.8}Mg_{0.2}O_3$ electrolyte membranes for intermediate-temperature solid oxide fuel cells. *J. Mater. Chem. A* **2015**, *3*, 7535–7553.

[21] Song, Y. F.; Chen, Y. B.; Xu, M. G.; Wang, W.; Zhang, Y.; Yang, G. M.; Ran, R.; Zhou, W.; Shao, Z. P. A cobalt-free multi-phase nanocomposite as near-ideal cathode of intermediate-temperature solid oxide fuel cells developed by smart self-assembly. *Adv. Mater.* **2020**, *32*, 1906979.

[22] Cowin, P. I.; Petit, C. T. G.; Lan, R.; Irvine, J. T. S.; Tao, S. W. Recent progress in the development of anode materials for solid oxide fuel cells. *Adv. Energy Mater.* **2011**, *1*, 314–332.

[23] Duan, C. C.; Tong, J. H.; Shang, M.; Nikodemski, S.; Sanders, M.; Ricote, S.; Almansoori, A.; O'Hayre, R. Readily processed protonic ceramic fuel cells with high performance at low temperatures. *Science* **2015**, *349*, 1321–1326.

[24] Cao, J. F.; Jia, Y. X.; Shao, Z. P. Perovskites for protonic ceramic fuel cells: A review. *Energy Environ. Sci.* **2022**, *15*, 2200–2232.

[25] Ferguson, K.; Dubois, A.; Albrecht, K.; Braun, R. J. High performance protonic ceramic fuel cell systems for distributed power generation. *Energy Convers. Manag.* **2021**, *248*, 114763.

[26] Seong, A.; Kim, J.; Jeong, D.; Sengodan, S.; Liu, M. L.; Choi, S.; Kim, G. Electrokinetic proton transport in triple ($H^+/O^{2-}/e^-$)

conducting oxides as a key descriptor for highly efficient protonic ceramic fuel cells. *Adv. Sci.* **2021**, *8*, 2004099.

[27] Hu, D. Y.; Kim, J.; Niu, H. J.; Daniels, L. M.; Manning, T. D.; Chen, R. Y.; Liu, B. W.; Feetham, R.; Claridge, J. B.; Rosseinsky, M. J. High-performance protonic ceramic fuel cell cathode using protophilic mixed ion and electron conducting material. *J. Mater. Chem. A* **2022**, *10*, 2559–2566.

[28] Lv, X. Q.; Chen, H. L.; Zhou, W.; Li, S. D.; Shao, Z. P. A CO_2-tolerant $SrCo_{0.8}Fe_{0.15}Zr_{0.05}O_{3-\delta}$ cathode for proton-conducting solid oxide fuel cells. *J. Mater. Chem. A* **2020**, *8*, 11292–11301.

[29] Zhou, C.; Sunarso, J.; Song, Y. F.; Dai, J.; Zhang, J. X.; Gu, B. B.; Zhou, W.; Shao, Z. P. New reduced-temperature ceramic fuel cells with dual-ion conducting electrolyte and triple-conducting double perovskite Cathode. *J. Mater. Chem. A* **2019**, *7*, 13265–13274.

[30] Liu, M. F.; Gao, J. F.; Liu, X. Q.; Meng, G. Y. High performance of anode supported $BaZr_{0.1}Ce_{0.7}Y_{0.2}O_{3-\delta}$ (BZCY) electrolyte cell for IT-SOFC. *Int. J. Hydrogen Energ* **2011**, *36*, 13741–13745.

[31] Xu, X.; Wang, H. Q.; Fronzi, M.; Wang, X. F.; Bi, L.; Traversa, E. Tailoring cations in a perovskite cathode for proton-conducting solid oxide fuel cells with high performance. *J. Mater. Chem. A* **2019**, *7*, 20624–20632.

[32] Shimada, H.; Yamaguchi, Y.; Sumi, H.; Mizutani, Y. Performance comparison of perovskite composite cathodes with $BaZr_{0.1}Ce_{0.7}Y_{0.1}Yb_{0.1}O_{3-\delta}$ in anode-supported protonic ceramic fuel cells. *J. Electrochem. Soc.* **2020**, *167*, 124506.

[33] Zhu, Z. W.; Qian, J.; Wang, Z. T.; Dang, J. J.; Liu, W. High-performance anode-supported solid oxide fuel cells based on nickel-based cathode and $Ba(Zr_{0.1}Ce_{0.7}Y_{0.2})O_{3-\delta}$ electrolyte. *J. Alloys Compd.* **2013**, *581*, 832–835.

[34] Zhang, Y.; Chen, B.; Guan, D. Q.; Xu, M. G.; Ran, R.; Ni, M.; Zhou, W.; O'Hayre, R.; Shao, Z. P. Thermal-expansion offset for high-performance fuel cell cathodes. *Nature* **2021**, *591*, 246–251.

[35] Thaheem, I.; Kim, K. J.; Lee, J. J.; Joh, D. W.; Jeong, I.; Lee, K. T. High performance $Mn_{1.3}Co_{1.3}Cu_{0.4}O_4$ spinel based composite cathodes for intermediate temperature solid oxide fuel cells. *J. Mater. Chem. A* **2019**, *7*, 19696–19703.

[36] Xu, Y. J.; Wen, Z. Y.; Wang, S. R.; Wen, T. L. Cu doped Mn-Co spinel protective coating on ferritic stainless steels for SOFC interconnect applications. *Solid State Ionics* **2011**, *192*, 561–564.

[37] Shao, L.; Wang, Q.; Fan, L. S.; Wang, P. X.; Zhang, N. Q.; Sun, K. N. Copper cobalt spinel as a high performance cathode for intermediate temperature solid oxide fuel cells. *Chem. Commun.* **2016**, *52*, 8615–8618.

[38] Zhen, S. Y.; Sun, W.; Li, P. Q.; Tang, G. Z.; Rooney, D.; Sun, K. N.; Ma, X. X. High performance cobalt-free $Cu_{1.4}Mn_{1.6}O_4$ spinel oxide as an intermediate temperature solid oxide fuel cell cathode. *J. Power Sources* **2016**, *315*, 140–144.

[39] Zhang, X. M.; Liu, L.; Zhao, Z.; Shang, L.; Tu, B. F.; Ou, D. R.; Cui, D. A.; Cheng, M. J. High performance solid oxide fuel cells with $Co_{1.5}Mn_{1.5}O_4$ infiltrated (La, Sr)MnO_3-yittria stabilized zirconia cathodes. *Int. J. Hydrogen Energy* **2015**, *40*, 3332–3337.

[40] Jiang, S. S.; Sunarso, J.; Zhou, W.; Shao, Z. P. The significant effect of the phase composition on the oxygen reduction reaction activity of a layered oxide cathode. *J. Mater. Chem. A* **2013**, *1*, 11026–11032.

[41] Wan, T. H.; Saccoccio, M.; Chen, C.; Ciucci, F. Influence of the discretization methods on the distribution of relaxation times deconvolution: Implementing radial basis functions with DRTtools. *Electrochim. Acta* **2015**, *184*, 483–499.

[42] Song, Y. F.; Chen, Y. B.; Wang, W.; Zhou, C.; Zhong, Y. J.; Yang, G. M.; Zhou, W.; Liu, M. L.; Shao, Z. P. Self-assembled triple-conducting nanocomposite as a superior protonic ceramic fuel cell cathode. *Joule* **2019**, *3*, 2842–2853.

[43] Zou, D.; Yi, Y. N.; Song, Y. F.; Guan, D. Q.; Xu, M. G.; Ran, R. Wang, W.; Zhou, W.; Shao, Z. P. The $BaCe_{0.16}Y_{0.04}Fe_{0.8}O_{3-\delta}$ nanocomposite: A new high-performance cobalt-free triple-conducting cathode for protonic ceramic fuel cells operating at reduced temperatures. *J. Mater. Chem. A* **2022**, *10*, 5381–5390.

[44] Gu, H. X.; Su, C.; Zhou, C.; Liu, Y.; Zhang, Y.; Yang, G. M.; Zhou, W.; Shao, Z. P. $LaBa_{0.8}Ca_{0.2}Co_2O_{5+\delta}$ cathode with superior CO_2 resistance and high oxygen reduction activity for intermediate-temperature solid oxide fuel cells. *Int. J. Hydrogen Energy* **2022**, *47*, 16214–16221.

[45] Xu, Y. S.; Xu, X.; Bi, L. A high-entropy spinel ceramic oxide as the cathode for proton-conducting solid oxide fuel cells. *J. Adv. Ceram.* **2022**, *11*, 794–804.

[46] Gu, H. X.; Sunarso, J.; Yang, G. M.; Zhou, C.; Song, Y. F.; Zhang, Y.; Wang, W.; Ran, R.; Zhou, W.; Shao, Z. P. Turning detrimental effect into benefits: Enhanced oxygen reduction reaction activity of cobalt-free perovskites at intermediate temperature via CO_2-induced surface activation. *ACS Appl. Mater. Interfaces* **2020**, *12*, 16417–16425.

[47] Wang, M.; Su, C.; Zhu, Z. H.; Wang, H.; Ge, L. Composite cathodes for protonic ceramic fuel cells: Rationales and materials. *Composites Part B: Eng.* **2022**, *238*, 109881.

[48] Ren, R. Z.; Wang, Z. H.; Xu, C. M.; Sun, W.; Qiao, J. S.; Rooneyc, D. W.; Sun, K. N. Tuning the defects of the triple conducting oxide $BaCo_{0.4}Fe_{0.4}Zr_{0.1}Y_{0.1}O_{3-\delta}$ perovskite toward enhanced cathode activity of protonic ceramic fuel cells. *J. Mater. Chem. A* **2019**, *7*, 18365–18372.

[49] Tong, H.; Fu, M.; Yang, Y.; Chen, F. L.; Tao, Z. T. A novel self-assembled cobalt-free perovskite composite cathode with triple-conduction for intermediate proton-conducting solid oxide fuel cells. *Adv. Funct. Mater.* **2022**, *32*, 2209695.

[50] Fan, L. D.; Su, P. C. Layer-structured $LiNi_{0.8}Co_{0.2}O_2$: A new triple ($H^+/O^{2-}/e^-$) conducting cathode for low temperature proton conducting solid oxide fuel cells. *J. Power Sources* **2016**, *306*, 367–377.

[51] Taillades, G.; Pers, P.; Mao, V.; Taillades, M. High performance anode-supported proton ceramic fuel cell elaborated by wet powder spraying. *Int. J. Hydrogen Energy* **2016**, *41*, 12330–12336.

[52] Cui, J. J.; Wang, J. K.; Zhang, X. W.; Li, G. J.; Wu, K.; Cheng, Y. H.; Zhou, J. Enhanced oxygen reduction reaction through Ca and Co co-doped $YFeO_3$ as cathode for protonic ceramic fuel cells. *J. Power Sources* **2019**, *413*, 148–157.

[53] Wei, K. W.; Li, N.; Wu, Y. J.; Song, W. C.; Wang, X. X.; Guo, L. T.; Khan, M.; Wang, S. R.; Zhou, F. B.; Ling, Y. H. Characterization and optimization of highly active and Ba-deficient $BaCo_{0.4}Fe_{0.4}Zr_{0.1}Y_{0.1}O_{3-\delta}$-based cathode materials for protonic ceramics fuel cells. *Ceram. Int.* **2019**, *45*, 18583–18591.

[54] Xie, D.; Ling, A.; Yan, D.; Jia, L. C.; Chi, B.; Pu, J.; Li, J. A comparative study on the composite cathodes with proton conductor and oxygen ion conductor for proton-conducting solid oxide fuel cell. *Electrochim. Acta* **2020**, *344*, 136143.

[55] Sun, S. C.; Cheng, Z. $SrCo_{0.8}Nb_{0.1}Ta_{0.1}O_{3-\delta}$ based cathodes for electrolyte-supported proton-conducting solid oxide fuel cells: Comparison with $Ba_{0.5}Sr_{0.5}Co_{0.8}Fe_{0.2}O_{3-\delta}$ based cathodes and implications. *J. Electrochem. Soc.* **2020**, *167*, 024514.

[56] Xie, D.; Li, K.; Yang, J.; Yan, D.; Jia, L. C.; Chi, B.; Pu, J.; Li, J. High-performance $La_{0.5}(Ba_{0.75}Ca_{0.25})_{0.5}Co_{0.8}Fe_{0.2}O_{3-\delta}$ cathode for proton-conducting solid oxide fuel cells. *Int. J. Hydrogen Energy* **2021**, *46*, 10007–10014.

[57] Seong, A.; Jeong, D.; Kim, M.; Choi, S.; Kim, G. Performance comparison of composite cathode: Mixed ionic and electronic conductor and triple ionic and electronic conductor with $BaZr_{0.1}Ce_{0.7}Y_{0.1}Yb_{0.1}O_{3-\delta}$ for highly efficient protonic ceramic fuel cells. *J. Power Sources* **2022**, *530*, 231241.

[58] Shi, H. G.; Su, C.; Xu, X. M.; Pan, Y. L.; Yang, G. M.; Ran, R.; Shao, Z. P. Building Ruddlesden–Popper and single perovskite nanocomposites: A new strategy to develop high-performance cathode for protonic ceramic fuel cells. *Small* **2021**, *17*, 2101872.

[59] Chen, J. Y.; Li, J.; Jia, L. C.; Moussa, I.; Chi, B.; Pu, J.; Li, J. A novel layered perovskite $Nd(Ba_{0.4}Sr_{0.4}Ca_{0.2})Co_{1.6}Fe_{0.4}O_{5+\delta}$ as cathode for proton-conducting solid oxide fuel cells. *J. Power Sources* **2019**, *428*, 13–19.

[60] Wang, D.; Xia, Y. P.; Lv, H. L.; Miao, L. N.; Bi, L.; Liu, W. $PrBaCo_{2-x}Ta_xO_{5+\delta}$ based composite materials as cathodes for proton-conducting solid oxide fuel cells with high CO_2 resistance. *Int. J. Hydrogen Energy* **2020**, *45*, 31017–31026.

[61] Liang, M. Z.; Zhu, Y. J.; Song, Y. F.; Guan, D. Q.; Luo, Z. X.; Yang, G. M.; Jiang, S. P.; Zhou, W.; Ran, R.; Shao, Z. P. A new durable surface nanoparticles-modified perovskite cathode for protonic

ceramic fuel cells from selective cation exsolution under oxidizing atmosphere. *Adv. Mater.* **2022**, *34*, 2106379.

[62] Liu, S. L.; Wu, M. L.; Lu, L. Y.; Ni, J. P.; Ni, C. S.; Irvine, J. T. S. $La_{0.5}Ba_{0.5}Cu_xFe_{1-x}O_{3-\delta}$ as cathode for high-performance proton-conducting solid oxide fuel cell. *Sep. Purif. Technol.* **2022**, *297*, 121485.

[63] Wang, Z.; Lv, P. F.; Yang, L.; Guan, R.; Jiang, J. D.; Jin, F. J.; He, T. M. $Ba_{0.95}La_{0.05}Fe_{0.8}Zn_{0.2}O_{3-\delta}$ cobalt-free perovskite as a triple-conducting cathode for proton-conducting solid oxide fuel cells. *Ceram. Int.* **2020**, *46*, 18216–18223.

[64] Ling, Y.; Zhao, L.; Liu, X.; Lin, B. Tailoring electrochemical property of layered perovskite cathode by Cu-doping for proton-conducting IT-SOFCs. *Fuel Cells* **2015**, *15*, 384–389.

[65] Liu, J. J.; Ding, J. W.; Miao, L. N.; Gong, Z.; Li, K.; Liu, W. High performance $Ba_{0.95}Ca_{0.05}Fe_{0.9-x}Sn_xY_{0.1}O_{3-\delta}$-SDC as cobalt-free cathode for intermediate-temperature proton-conducting solid oxide fuel cells with $BaZr_{0.1}Ce_{0.7}Y_{0.2}O_{3-\delta}$ electrolyte. *J. Alloys Compd.* **2019**, *786*, 163–168.

[66] Ma, Z. L.; Ye, Q. R.; Zhang, B. K.; Yang, W. Y.; Dong, F. F.; Ni, M.; Lin, Z. A highly efficient and robust bifunctional perovskite-type air electrode with triple-conducting behavior for low-temperature solid oxide fuel cells. *Adv. Funct. Mater.* **2022**, *32*, 2209054.